A numerical continuation approach using monodromy to solve the forward kinematics of cable-driven parallel robots with sagging cables

Aravind Baskar[a], Mark Plecnik[a], Jonathan D. Hauenstein[a], Charles W. Wampler[a]

[a] *University of Notre Dame, Notre Dame, 46556, Indiana, USA*

Abstract

Designing and analyzing large cable-driven parallel robots (CDPRs) for precision tasks is challenging because their position kinematics are governed by kineto-statics and cable sag equations. Our aim is to find all equilibria for a given set of unstrained cable lengths. The Irvine sagging cable model contains both non-algebraic and multi-valued functions. The former removes the guarantee that the number of solutions will be finite, making homotopy start system construction less clear. The latter introduces branch cuts, which should be minded during path tracking to avoid numerical failures. We reformulate the Irvine model to eliminate multi-valued functions and propose a heuristic numerical continuation method based on monodromy, which does not rely on sophisticated start systems. We demonstrate this approach on an eight-cable spatial CDPR, resulting in a non-algebraic system with a dimension of 31. Our findings show an increase of up to 50% in the number of solutions compared to existing data sets. This is expected to enhance the quality of these data sets for training neural network models in CDPR kineto-statics.

Keywords: Cable-driven parallel robot, Numerical continuation, Irvine cable model, Monodromy

1. Introduction

Cable-driven parallel robots (CDPRs) are a class of parallel manipulators in which an end-effector platform is controlled by multiple cables, whose lengths are adjusted to control its movements. These robots have proven effective for various applications, including visual sensing and manipulation in vast environments such as agricultural fields, sports stadiums, and theaters. Recently, there has been a resurgence of interest in designing CDPRs for precision tasks, such as 3D printing of large models [1, 2], construction robotics [3], and search and rescue missions [4]. Designing CDPRs for such tasks poses an ongoing research challenge due to the inherent complexity of their kinematics compared to traditional parallel robots with rigid legs. To ensure stability, cable-driven systems often require redundant cables to fully constrain the end-effector platform [5, 6], which complicates their analysis and design.

Unlike rigid links, cables are elastic and subject to sagging, making kinematic analysis inherently coupled with static equilibrium analysis, falling under the category of kineto-statics problems. The widely used Irvine cable model, which accounts for elasticity and sagging under self-weight [7, 8], is more realistic than simplified models that assume inelasticity and negligible mass [9, 10, 11]. Recent experimental research has highlighted the inadequacy of such simplified models for designing and analyzing large CDPRs [4, 12]. Consequently, many recent studies address kineto-static problems in cable-driven robots using the comprehensive Irvine cable model [13]. Unfortunately, this model involves multi-valued inverse hyperbolic and square-root functions which introduce branch cuts. At branch cuts, the system is non-analytic. If ignored, these branch cuts will lead to numerical failures during homotopy path tracking. By analytic, we refer to *complex-analytic* functions which are complex differentiable in a neighbourhood of every point in the entire complex domain [14, p. 69]. In contrast to the algebraic form of the simplified models, the nature of the Irvine cable model precludes the use of powerful algorithms specialized to algebraic systems.

Our goal is to solve the forward (a.k.a. direct) kineto-static equilibrium problem for CDPRs to find all solutions. That is, given a specific CDPR architecture with prescribed unstrained cable lengths, we seek to find all possible static equilibrium configurations . This is significantly harder than finding a single equilibrium configuration, which can be achieved using Newton's method with appropriate initial guesses. Solving the global forward kinematics is crucial for characterizing the comprehensive workspace of these

systems, which consists of numerous input modes separated by special configurations known as input singularities [15], sometimes called Type II singularities [16] or direct kinematic singularities [17, 18]. In parallel linkage systems, inverse kinematic problems involve determining the actuator inputs for a given end-effector pose. These problems are often simpler to solve, providing a quick means to sample and characterize the workspace. However, this approach is not straightforward in cable-driven parallel systems. The presence of redundant cables in CDPRs leads to a positive dimensional family of solutions to the inverse kinematic problem, introducing additional challenges in characterizing the workspace.

Finding all equilibria over a set of input sample points is necessary to have representatives of all input modes. The input modes may change over the input space, so we solve each sample in a sample set. Once a sufficient sample set has been created, local methods may be used to continue the solutions to nearby points. This process generates an extensive data set representing the workspace, which serves as the basis for training neural network models in the field of kineto-statics [19, 20]. Thus, solving the global forward kinematic problem is a key step in generating such data sets and is the focus of this research.

While one expects the roots to be isolated, i.e., zero-dimensional, it cannot be assumed in general that the total number of roots is finite due to the non-algebraic nature of the Irvine cable model. This is especially evident in the case of roots over the complex field. However, certain non-algebraic systems are known to yield a finite number of isolated roots over the real field when they contain *Pfaff functions* [21] (also called Pfaffian functions). Pfaff functions are a class of functions that can be written as polynomial functions of their own derivatives and other Pfaff functions. Polynomials, exponentials, and trigonometric functions are Pfaff functions that give rise to Pfaff manifolds over some open real domain. The inverse of a Pfaff function is also a Pfaff function if it does not vanish anywhere within the domain. The kineto-static equations of CDPRs with sagging cables give rise to these manifolds and, hence, the number of real roots must be finite even though the Irvine cable model is non-algebraic.

In the past, interval search methods which exploit appropriately chosen bounds on end-effector configuration and cable tension have been employed to solve the global forward kinematic problem in cable-driven robots [11, 22]. While interval search methods have demonstrated effectiveness in finding multiple instances, they face challenges as the number of cables controlling the end-effector increases. For instance, in a spatial system with eight cables, explored in [22], the search space encompassed 36 dimensions, and a single case required approximately 24 hours to solve. Additionally, it remains nearly impossible to ascertain whether all feasible configurations have been identified, even within predefined boundaries.

Alternatively, numerical algebraic geometry techniques have been employed by researchers to solve forward kinematics for rigid-legged parallel manipulators, involving the resolution of multivariate polynomial systems [23, 24]. In [25], kineto-statics of a compliant parallel manipulator with spring elements was addressed by solving a large polynomial system in a similar manner. Typically, numerical polynomial continuation techniques operate through a continuous transformation from a known starting polynomial system to a target polynomial system where the endpoints need to be determined. This is achieved through *path tracking* which defines paths one must track from the start points of the starting system to the endpoints of the target system. This method effectively addresses the challenge of solving moderately large polynomial systems completely. Numerical continuation techniques are often compared to other less sophisticated analytical methods, such as the multi-start Newton's method, which may identify numerous distinct root instances. Numerous studies involving large systems of nonlinear equations [26, 27] demonstrate that numerical continuation methods more efficiently exploit complex-analytic functions in comparison to multi-start Newton approaches. This efficiency is attributed to the guarantee that distinct starting points will lead to distinct endpoints, particularly when path crossings are absent.

To effectively employ numerical continuation techniques, a global assumption of complex-analyticity in functions is essential. However, in the case of the Irvine cable model, analyticity breaks down at the branch cuts introduced by inverse hyperbolic sines and square-roots. These multi-valued functions require the introduction of branch cuts, necessary discontinuities chosen by convention to yield a *principal* value over the complex domain [14, pp. 69-71]. In the absence of specific measures, such as switching branches when required, these discontinuities in function definitions can cause numerical continuation paths to fail when encountered. An additional challenge is constructing an appropriate start system for non-algebraic systems that may not possess a finite upper bound on the total number of roots. In particular in [28], a parameter continuation technique was used to progressively transform an inelastic taut cable system, which can be modeled as a polynomial system, into a sagging cable system. However, limited success was achieved

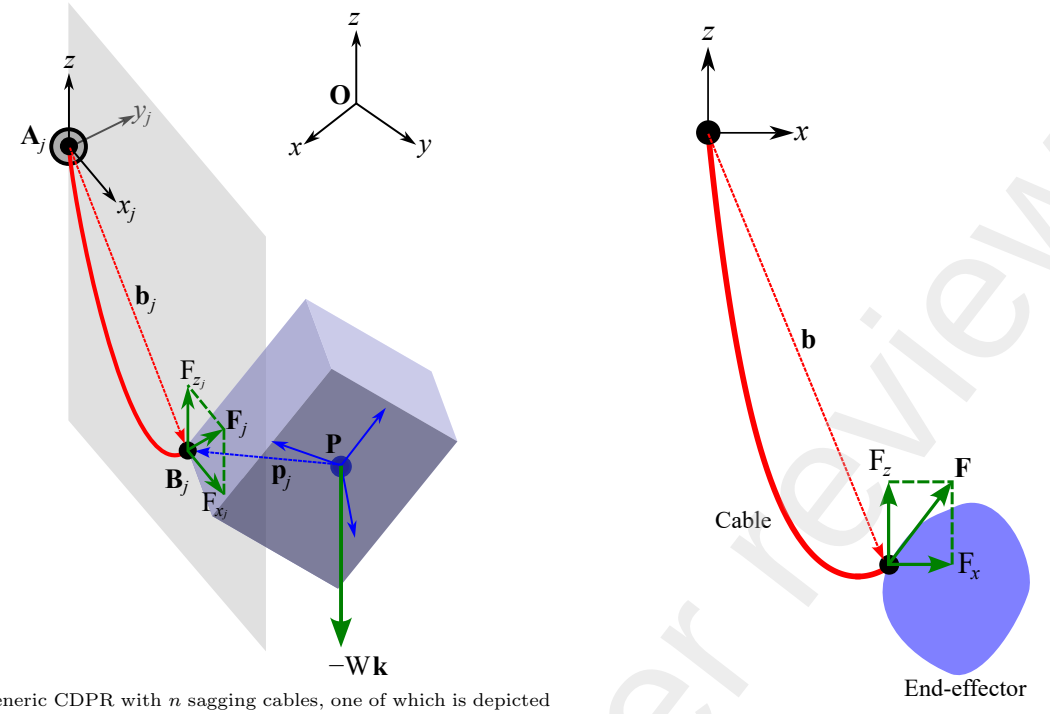

(a) A generic CDPR with n sagging cables, one of which is depicted in its vertical plane.

(b) Irvine sagging cable model in plane.

Figure 1: Schematic of a cable-driven parallel robot

due to significant failures reported during path tracking. Another shortcoming stems from the fact that a starting system constructed based on a simplified model cannot guarantee the capture of all roots of a full model target system, even if all paths were to be successful. Because of these two shortcomings, numerical continuation was considered insufficient for solving the global CDPR forward kinematic problem.

In this work, we propose a new continuation methodology that overcomes the two faults described above. First, we reformulate the Irvine cable model to remove multi-valued functions through a change of variables. This adaptation enables the utilization of numerical continuation as a viable solution technique. In theory, the occurrence of path failures can be almost completely avoided by conducting parameter continuation over the complex field [23]. Secondly, for solving non-algebraic systems, especially Pfaff equations, we introduce a heuristic root accumulation strategy using monodromy loops, eliminating the necessity for a start system. Using this algorithm, we demonstrate that the forward kinematics of large CDPRs with sagging cables can be solved more effectively, resulting in an increase of up to 50% in the number of equilibrium configurations compared to existing interval search and sampling methods. We present numerical examples and benchmark the results against an existing data set from the literature for an eight-cable spatial CDPR system [22, 29]. This method holds significant potential for generating comprehensive workspace data sets for CDPRs, which can be utilized for both training and testing neural networks of the kineto-static model.

2. Mathematical model of kineto-statics of a generic CDPR with n cables

Consider the schematic of a generic spatial CDPR with n cables as shown in Fig. 1a. Gravity acts downwards along the z-direction, $\hat{\mathbf{k}} = \{0, 0, 1\}^\top$. The end-effector is operated by n-cables, $j = 1, 2, \ldots, n$. Let $\mathbf{P} = (P_x, P_y, P_z)^\top$ be the position of the end-effector platform's center of mass in the global coordinate frame. The weight of the platform is $W = Mg$, where M is the mass of the end-effector platform and g the acceleration due to gravity. We assume no other external load in this work. The local frame of the end-effector is affixed to $\mathbf{P}$. Position vector $\mathbf{p}_j$ represents cable j connection point on the end-effector in the local frame of the end-effector. Let the orientation of the end-effector in the global coordinate frame be given by a 3×3 rotation matrix $[\mathbf{Q}]$. We use quaternion parameters $\{q_0, q_1, q_2, q_3\}$ to represent the 3×3

rotation matrix $[\mathbf{Q}]$ as follows:

$$[\mathbf{Q}] = \begin{bmatrix} {q_0}^2 + {q_1}^2 - {q_2}^2 - {q_3}^2 & 2\left(q_1 q_2 + q_0 q_3\right) & 2\left(-q_0 q_2 + q_1 q_3\right) \\ 2\left(q_1 q_2 - q_0 q_3\right) & {q_0}^2 - {q_1}^2 + {q_2}^2 - {q_3}^2 & 2\left(q_0 q_1 + q_2 q_3\right) \\ 2\left(q_0 q_2 + q_1 q_3\right) & 2\left(-q_0 q_1 + q_2 q_3\right) & {q_0}^2 - {q_1}^2 - {q_2}^2 + {q_3}^2 \end{bmatrix},$$

along with a normalization constraint:

$${q_0}^2 + {q_1}^2 + {q_2}^2 + {q_3}^2 = 1. \tag{1}$$

2.1. Position loop-closure equations

The j^{th} cable's fixed point is located at $\mathbf{A}_j$. Each cable can be assumed to lie in a vertical plane $X_j Z$ under static equilibrium conditions. Let the cable plane be at a z-rotation of ϕ_j which is represented as $[\mathbf{Z}(\phi_j)]$ with respect to the global coordinate plane XZ. Note that a z-rotation of $\phi_j + \pi$ also represents the same cable vertical plane with opposing x axes. The span of the j^{th} cable from its fixed point to the moving platform is represented by a local vector within the cable plane named $\mathbf{b}_j$. The position loop-closure equation associated with cable $j = 1, 2, \ldots, n$ is:

$$\mathbf{P} + [\mathbf{Q}]\ \mathbf{p}_j - [\mathbf{Z}(\phi_j)]\ \mathbf{b}_j - \mathbf{A}_j = \mathbf{0}, \tag{2}$$

where $\mathbf{b}_j$ is of the form $(b_{xj}, 0, b_{zj})^\top$ and given by the Irvine cable model in the local vertical cable plane in terms of the corresponding tension force $\mathbf{F}_j$ of the form $(F_{xj}, 0, F_{zj})^\top$. In the following, we revisit this model in detail and derive an equivalent representation made of complex-analytic functions which are amenable for numerical continuation methods.

Irvine cable model

Consider the schematic of a cable in the vertical plane XZ as shown in Fig. 1b. Let the coiling system of the cable be assumed at the origin of the cable vertical plane. Acceleration due to gravity g is downwards along the z-direction. We neglect all lateral static forces on the cable, so the cable lies in a vertical plane. The cable stretches under tension and sags under self-weight. Let ρ, A and E be the properties of the cables, namely, linear density, cross sectional area, and Young's modulus, respectively. According to the Irvine model [7], the kineto-statics equations for a cable of unstrained length L are:

$$\mathbf{b} = \begin{pmatrix} b_x \\ 0 \\ b_z \end{pmatrix} = \begin{pmatrix} F_x \left(\frac{L}{EA} + \frac{1}{\rho g} \left(\sinh^{-1}\left[\frac{F_z}{F_x}\right] - \sinh^{-1}\left[\frac{F_z - \rho g L}{F_x}\right] \right) \right) \\ 0 \\ \frac{F_z L}{EA} - \frac{\rho g L^2}{2EA} + \frac{1}{\rho g} \left(\sqrt{{F_x}^2 + {F_z}^2} - \sqrt{{F_x}^2 + \left(F_z - \rho g L\right)^2} \right) \end{pmatrix}, \tag{3}$$

where $\mathbf{F} = (F_x, F_z)^\top$ is the tension in the cable at its end, resolved into horizontal and vertical components in the cable vertical plane. The y-coordinates of tension and position are both zero by assumption. Here, $F_x > 0$ is a necessary operating condition of the Irvine model for the cable to be in tension and hence, $b_x > 0$. A mirrored configuration with $b_x < 0$ can be ignored, because it is already accounted for in a z-rotation of the cable vertical plane by π as noted earlier.

Eq. (3) contains branch cuts because of the presence of the inverse hyperbolic sine and square-root functions which are multi-valued over the complex domain. Branch cuts are defined by convention for a principal definition. See Fig. 2 for one possible such definition for these functions involving branch-cuts (shown in blue). In the case of the square-root function, a branch cut is conventionally defined in most programming libraries along the negative real axis $(-\infty, 0)$, while it is defined along the imaginary axis $(-i\infty, -i)$ and $(i, i\infty)$ for the inverse hyperbolic sine function. (Note that the apparent discontinuity along the negative real axis in Fig. 2b is not a branch cut: it arises due to limitations in visualizing the complex argument.) If these standard definitions are used, the branch cuts cause failures during numerical continuation whenever a path crosses one of these discontinuities. Unless special branch switching logic is implemented, any robust predictor-corrector path-tracking algorithm slows down indefinitely upon the

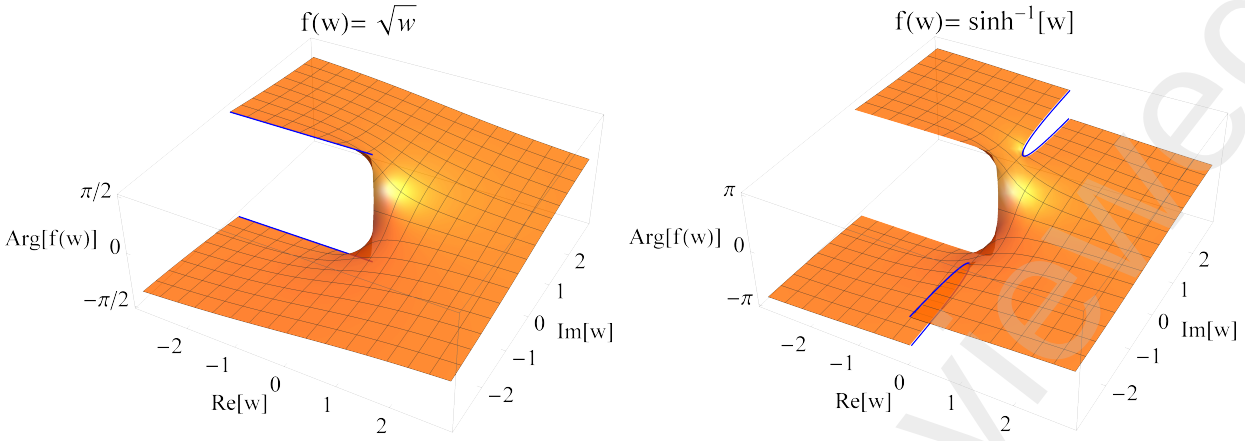

(a) Square-root function $f(w) = \sqrt{w}$

(b) Inverse hyperbolic sine function $f(w) = \sinh^{-1}[w]$

Figure 2: Principal branch of multi-valued functions of a complex variable w defined using branch cuts

approach of such cuts and eventually grinds to a halt upon reaching the maximum number of steps. These failures do not manifest in the form of ill-conditioning.

Illustration: Consider a simple homotopy equation, $H(w[t], t) := w[t] - \sqrt{e^{2\pi i t}} = 0$, from $t = 0$ to $t = 1$ with a start point $w[0] = 1$, where $\sqrt{\cdot}$ is the principal square-root function. Solving this equation using any certified predictor-corrector tracking algorithm fails as $t \to 0.5^-$ where the path encounters a branch-cut of the principal square-root function along the negative real axis at -1. Note that $\lim_{t\to 0.5^-} w'[t] = -\pi \neq 0$. Thus it is not a *path crossing* failure which are typically caused by system singularities where at least two solution branches of w merge. One way to circumvent this implementation problem is by keeping track of the sheet of the multi-valued function we are on currently by introducing additional variables. In the square-root example, it can also be achieved by modifying the homotopy via squaring as $H(w[t], t) := w[t]^2 - e^{2\pi i t} = 0$. While this resolves the analyticity issue allowing us to track until $t = 1$, it introduces a second branch with a corresponding start point $w[0] = -1$. This is an unavoidable cost of resolving analyticity.

In a previous work on the kinematics of cable-driven parallel robots using a numerical continuation approach [28], several path failures were reported which could not be adequately explained by the condition number of the local Jacobian matrix. The illustration above explains one such scenario caused by branch cuts. The presence of multi-valued functions must be addressed before effective numerical homotopy path tracking can proceed. Numerical continuation carried out over the real parameter space does not resolve the analyticity issue either for the following reasons: 1) While the hyperbolic sine function is *bijective* over the real domain, the square-root function has a branch point at the origin to contend with even over the reals. 2) Path crossings due to system singularities bog down real parameter continuation computations.

Change of variables

To effectively apply numerical continuation, we need to reformulate the Irvine cable model to get rid of the square-root function and the inverse hyperbolic sine function. To do so, we introduce a change of variables from F_x, F_z to new real variables α, β:

$$\frac{F_z}{F_x} = \sinh[\alpha], \quad \frac{F_z - \rho g L}{F_x} = \sinh[\beta]. \tag{4}$$

Assuming $\rho > 0$ and $L > 0$, F_x and F_z can be expressed in terms of the new variables α and β:

$$F_x = \frac{\rho g L}{\sinh[\alpha] - \sinh[\beta]}, \quad F_z = \frac{\rho g L \sinh[\alpha]}{\sinh[\alpha] - \sinh[\beta]}. \tag{5}$$

The next-step is to re-write the square-root functions in the Irvine model given by Eq. (3) in terms of the new variables. First consider the following expression:

$$F_x{}^2 + F_z{}^2 = \frac{\rho^2 g^2 L^2 \cosh^2[\alpha]}{(\sinh[\alpha] - \sinh[\beta])^2}.$$

The numerator is always a square of a positive number ($\because \cosh[a] \geq 1,\ \forall\ a \in \mathbb{R}$), but the same is not generically true for the denominator. However, Irvine cable model requires $F_x > 0$ which translates to $\sinh[\alpha] > \sinh[\beta]$ based on the definition in Eq. (5). Since the hyperbolic sine function is strictly increasing over $\mathbb{R}$, this condition reduces to $\alpha > \beta$. With this assumption, it follows that the real positive square-root:

$$\sqrt{{F_x}^2 + {F_z}^2} = \frac{\rho g L \cosh[\alpha]}{\sinh[\alpha] - \sinh[\beta]}. \tag{6}$$

Similarly, it can be easily shown that the real positive square-root:

$$\sqrt{{F_x}^2 + (F_z - \rho g L)^2} = \frac{\rho g L \cosh[\beta]}{\sinh[\alpha] - \sinh[\beta]}. \tag{7}$$

Substituting Eqs. (4-7) into Eq. (3):

$$\mathbf{b} = \begin{pmatrix} \frac{\rho g L}{\sinh[\alpha]-\sinh[\beta]} \left(\frac{L}{EA} + \frac{1}{\rho g} \left(\sinh^{-1}[\sinh[\alpha]] - \sinh^{-1}[\sinh[\beta]] \right) \right) \\ 0 \\ \frac{\sinh[\alpha]}{\sinh[\alpha]-\sinh[\beta]} \frac{\rho g L^2}{EA} - \frac{\rho g L^2}{2EA} + L \frac{\cosh[\alpha]-\cosh[\beta]}{\sinh[\alpha]-\sinh[\beta]} \end{pmatrix}.$$

Since hyperbolic sine function is bijective over $\mathbb{R}$,

$$\mathbf{b} = \begin{pmatrix} \frac{L}{\sinh[\alpha]-\sinh[\beta]} \left(\frac{\rho g L}{EA} + \alpha - \beta \right) \\ 0 \\ \frac{\sinh[\alpha]+\sinh[\beta]}{\sinh[\alpha]-\sinh[\beta]} \frac{\rho g L^2}{2EA} + L\ \frac{\cosh[\alpha]-\cosh[\beta]}{\sinh[\alpha]-\sinh[\beta]} \end{pmatrix}.$$

It can be observed that this modified kineto-static equation is a function of $\nu = \frac{\rho g}{EA}$, a combined material constant of the cable with units of reciprocal length. It defines the strain of a vertically hung cable under its self-weight normalized by its unstrained length.

Reformulated sagging cable model

In summary, through a change of variables from F_x, F_z to α, β under the assumption that $\rho > 0$ and $L > 0$, we propose an equivalent sagging cable model:

$$\mathbf{b} = \begin{pmatrix} b_x \\ 0 \\ b_z \end{pmatrix} = \frac{L}{\sinh[\alpha] - \sinh[\beta]} \begin{pmatrix} \nu\ L + \alpha - \beta \\ 0 \\ (\sinh[\alpha] + \sinh[\beta])\ \nu\ \frac{L}{2} + \cosh[\alpha] - \cosh[\beta] \end{pmatrix}, \tag{8}$$

where $\nu = \frac{\rho g}{EA}$. The corresponding cable tension in the vertical plane is given in Eq. (5). Equations (5,8) define the Irvine model in terms of the new real variables α, β with a necessary operating condition that $\alpha > \beta$. In some systems with metallic cables, it may be a reasonable approximation to neglect elasticity by setting $\nu \to 0$ as $E \to \infty$. This system is complex-analytic disregarding the inequality condition $\alpha > \beta$. Note that hyperbolic sine and cosine functions are single-valued over the complex domain. The equations cannot be made algebraic as they contain both algebraic and exponential forms of α and β. However, as noted earlier, this system defines Pfaff manifolds.

Note from Eq. (4) that the magnitudes of α and β grow in a slow *logarithmic* manner with respect to the ratio $\left|\frac{F_z}{F_x}\right|$. In addition to removing multi-valued functions, this new formulation may offer an advantage when numerically solving CDPR systems subjected to large magnitude forces. In particular, when the payload is suspended between horizontally taut cables so that $|F_x| \gg |F_z|$, the new variables α and β remain small in

magnitude. Although for brevity we omit a derivation, we note that the cable profile in the vertical plane can be derived in terms of the new variables, following [7], in parametric form $c \in [0, 1]$:

$$\frac{L}{\sinh[\alpha] - \sinh[\beta]} \begin{pmatrix} c\,\nu\,L + \sinh^{-1}\left[c\,\sinh[\alpha] + (1-c)\,\sinh[\beta]\right] - \beta \\ 0 \\ (c\,\sinh[\alpha] + (2-c)\,\sinh[\beta])\,c\,\nu\,\frac{L}{2} + \sqrt{1 + (c\,\sinh[\alpha] + (1-c)\,\sinh[\beta])^2} - \cosh[\beta] \end{pmatrix}, \tag{9}$$

where $c = 0$ corresponds to the origin of the cable and $c = 1$ corresponds to the end-effector connection point given by Eq. (8).

2.2. Force and torque equilibrium equations

With the relation between tension forces and cable displacement in hand, our next task is to form equations for force and torque balance. Let $\mathbf{F}_j = (F_{x_j}, 0, F_{z_j})^\top$ represent the tension force in cable j at the end-effector point. F_{x_j} and F_{z_j} are written in terms of the modified variables α_j and β_j following Eq. (5). Expressed in the world coordinate system, the sum of all forces on the end-effector including each cable reaction force $-\mathbf{F}_j$ and the weight of the platform $W = Mg$ acting along the negative z-direction gives the condition for force equilibrium:

$$\sum_{j=1}^{n} \left[\mathbf{Z}(\phi_j)\right](-\mathbf{F}_j) - W\hat{\mathbf{k}} = \mathbf{0}, \tag{10}$$

The torque equilibrium equations with respect to $\mathbf{P}$ are written as:

$$\sum_{j=1}^{n} \left([\mathbf{Q}]\ \mathbf{p}_j\right) \times \left(\left[\mathbf{Z}(\phi_j)\right](-\mathbf{F}_j)\right) = \mathbf{0}. \tag{11}$$

Assuming all cables have identical linear density, ρ, the force and the torque equilibrium equations can be simplified slightly by dividing out the constant ρg. Equations (1,2,10,11) amount to $1 + 3n + 3 + 3 = 3n + 7$ kineto-statics equations. For the forward kinematic problem, the variables are $\{\alpha_j, \beta_j, \phi_j\}$ for $j = 1, 2, \ldots, n$ along with the position of the center of mass $\mathbf{P}$ of the platform and the quaternion parameters $\{q_0, q_1, q_2, q_3\}$, which also totals to $3n + 7$ in number. For generic architecture parameters, this leads to a well-posed system of equations defining the forward kinematics.

2.3. Discussions

The following discussions on the mathematical model are pertinent:

1. The material constants of the kineto-statics system appear only as the ratios $\nu = \frac{\rho g}{EA}$ and $\lambda = \frac{W}{\rho g} = \frac{M}{\rho}$.
2. Over the complex field with imaginary unit i, one may see that if $\{\alpha_j, \beta_j, \phi_j\}$ satisfy Eqs. (2,10,11) so does $\{\alpha_j + i\pi N_1, \beta_j + i\pi N_1, \phi_j + \pi(N_1 + 2N_2)\}$, for any two integers N_1, N_2. These group actions derive from our reformulation to eliminate branch cuts in favor of *many-to-one* functions and the fact that every vertical plane has two z-rotational representations with respect to the global coordinate frame. Similar to the examples in [30, 31], these group actions also apply to the homotopy paths we consider, so we only track one member of each group. When recording roots, we consider subsequent occurrences of members of the same group as repeat instances, and in particular, for real roots, we record the principal representation with real-valued α_j, β_j and $\phi_j \in (-\pi, \pi]$.
3. The quaternion parameters admit two representations for any given $[\mathbf{Q}]$, namely, $\{q_0, q_1, q_2, q_3\}$ and $\{-q_0, -q_1, -q_2, -q_3\}$. Group action can be exploited in a similar manner as before.
4. A question remains on how best to involve the necessary inequality constraint, $\alpha_j > \beta_j,\ \forall\ j$. Handling this inequality upfront is cumbersome for an n-cable system because there arise n such inequalities and they cannot be evaluated over the complex field. More importantly, numerical continuation paths starting from a real root which violates these inequalities can result in a *valid* real root and vice versa. Hence, we ignore them during computations and compute all possible roots of the system including those which violate these inequalities. During post-processing, an additional check must be undertaken to identify the valid roots. Only those real roots which abide by the condition $\alpha_j > \beta_j,\ \forall\ j$ are the valid ones.

Remark on the planar case. When one applies this model to planar n-cable CDPRs, the number of variables can be reduced. For a system lying in the XZ-plane, the $[\mathbf{Q}]$ simplifies to only a y-rotation. The y-components of the position loop-closure equations as well as the force equilibrium equations identically vanish. The same is true for the x and z components of the torque equilibrium equations. Further, ϕ_j can only admit 0 or π for all $j = 1, 2, \ldots, n$ in the planar case. This results in 2^n sub-systems considering all combinations. Unexpectedly, these 2^n sub-systems are equivalent to each other because of the group action associated to N_1. For instance, a real solution with cable j in the form $\{\alpha_j, \beta_j, \pi\}$ also occurs as a complex one $\{\alpha_j + i\pi N_1, \beta_j + i\pi N_1, 0\}$ for odd N_1. Hence, it is sufficient to solve one of the 2^n sub-systems, for example, the one with $\phi_j = 0,\ \forall\ j$, in order to obtain all of the valid configurations.

3. Solving non-algebraic, complex-analytic systems via monodromy loops

In preparation for solving the global forward kinematic problem of CDPRs with sagging cables, we next propose a heuristic numerical continuation algorithm that exploits monodromy to solve non-algebraic, complex-analytic systems.

Numerical continuation is an effective technique to solve nonlinear system of equations which are complex-analytic in nature [32]. This technique works through predictor-corrector path tracking which continuously deforms the start point(s) of a known system into the end point(s) associated with a target system of interest. Specifically for finding all isolated roots of polynomial system of equations, theory on the construction of efficient start systems is well-developed exploiting the Bézout bounds [23, 24] as well as the sparse structure of these polynomial systems [33, 34]. For non-algebraic systems without any theoretical bounds on the number of roots, construction of efficient start systems for numerical continuation is an open research question. Start systems constructed through a simplified polynomial approximation of the original system is an option as done in [28] in the context of kinematics of CDPRs. However, if a simplified start system were to be used, there is no guarantee that all the target points of interest may be found.

In many polynomial systems which arise in kinematic design and analysis, it is noted that the actual number of roots is only a small fraction of the number of start points of a well-constructed start system, e.g., [35]. Most of the paths in such a homotopy diverge, making such methods computationally expensive in disproportion to the actual root-count. An increasingly popular approach for countering this effect is to abandon the construction of exhaustive start systems and instead implement heuristics that involve random processes with the goal of obtaining most or all solutions probabilistically [36], such as monodromy methods [31, 37, 38, 39]. *Monodromy* describes how roots of a parameterized system of equations change as loops are traced in the parameter space around branch points. Specifically, in a polynomial system that has a finite root-count, monodromy is a group action that permutes the set of all isolated roots as homotopy loops are traced along smooth paths in a parameter space. Given at least one root of the target system, one may seek to accumulate additional roots by tracking nontrivial monodromy loops, but it is difficult to know ahead of time which loops in parameter space will land on new roots versus which ones will return to roots already known. A well-tested root accumulation strategy is to execute random monodromy loops [39, 40]. Under certain assumptions of independence, the accumulation of roots follows the Lincoln-Petersen mark-and-recapture model, where the computational expense is roughly proportional to the total number of finite roots. This strategy does not generally extend to non-algebraic systems, as the total root count cannot be assumed finite, leading to a non-terminating algorithm. However, if such non-algebraic systems define Pfaff manifolds, the real root count is finite. Hence, modifications to the root accumulation strategy of the original random monodromy loops algorithm can be made by limiting it to finding and accepting only real roots while rejecting complex roots when they are encountered.

3.1. Random monodromy loops

In this section, we propose an algorithm that uses random monodromy loops with a heuristic root accumulation strategy to solve non-algebraic, complex-analytic systems. A common strategy in treating non-algebraic systems is to use a homotopy in which the parameter space is an array of constants added to the given system, for example, see the so-called Newton homotopies in [26, 41].

Consider a nonlinear complex-analytic system of equations $\mathbf{f}(\mathbf{w}) = \mathbf{0}$ of n equations in n unknowns, $\mathbf{w}$, for which numerical approximations of many or all real roots $\mathbf{w}$ are sought. We construct a parameter

homotopy with parameter array $\boldsymbol{\tau}$ of dimension n and path parameter $t \in \mathbb{R}$:

$$\mathbf{H}(\mathbf{w}[t], t) := \mathbf{f}(\mathbf{w}[t]) - \boldsymbol{\tau}(t), \tag{12}$$

where $\boldsymbol{\tau}(t)$ is defined such that $\boldsymbol{\tau}(0) = \mathbf{0}$. A random monodromy loop may be constructed then as:

$$\boldsymbol{\tau}(t) = \boldsymbol{\gamma}(1 - e^{2\pi i t}), \tag{13}$$

where $\boldsymbol{\gamma}$ is a random vector of non-zero complex numbers of dimension n. This circular monodromy loop is chosen for ease of implementation. (There exist other multi-nodal constructions such as a triangular segmented loop, petal shaped loop made of two different segments, etc., which may be equally preferable [42].) As t moves along the real line, every integer value gives $\boldsymbol{\tau}(t) = \mathbf{0}$, thereby leading $\mathbf{w}$ to a root of $\mathbf{f}(\mathbf{w}) = \mathbf{0}$. All solutions of $\mathbf{f}(\mathbf{w}) = \mathbf{0}$, including all real solutions, lie in the fiber over $\boldsymbol{\tau} = \mathbf{0}$, but for a fixed $\boldsymbol{\gamma}$, one cannot be assured that they all lie on one connected component. We may increase the chances of connecting to all real solutions by repeating the procedure using different random vectors $\boldsymbol{\gamma}$.

With this construction, we propose an algorithm for solving the problem, outlined as follows:

1. **Initialization**: We start by finding an initial starting solution $\mathbf{w}[0] = \mathbf{w}^*$ using a local Newton's method with an initial guess over the complex field. Note that finding a real starting root using Newton's method, while preferable, is non-trivial, especially in large systems. Hence we rely on complex starting roots. Care must be taken to ensure that the starting root satisfies the system of equations within a small tolerance, say 10^{-8}, and is also a non-singular root of the system with a singular value no smaller than, say 10^{-16}. To ensure robustness, we may repeat this step for up to 200 trials as required until a non-singular complex root is found. The algorithm allows for the possibility of starting with a user-defined initial point if it represents a good numerical approximation of a root.
2. **Monodromy Loop Tracking**: A random vector $\boldsymbol{\gamma}$ is initialized to define a monodromy loop for the current iteration. Using an adaptive step-size mixed precision (up to 32 decimal digits of precision) predictor-corrector tracking algorithm, we perform monodromy loops starting from $t = 0$ marching forward along the homotopy path. We employ a tracker similar to the ones proposed in [43, 44]. It uses a Padé predictor with numerator order 2 and denominator order 1, effective at navigating near path crossing scenarios, and a certified Newton's corrector with some adaptations to reduce step-size aggressively in case of step rejection. As the path variable t crosses a positive integer, we record the corresponding root and append only the real distinct ones among them to the list of start points. Retaining all the complex roots would quickly become unmanageable, because these tend to vastly outnumber the real roots. Care must be taken to ensure that duplicate instances are rejected, taking into account alternative representations according to group actions if any. Each path continues until one of the following criteria is met:
   - A circuit is completed, meaning that we return to the initial root $\mathbf{w}^*$.
   - A previously known real start point or an alternate member of its group is recorded.
   - A path fails due to numerical issues.
   - A path proceeds without yielding any real roots for m successive instances of t crossing a positive integer.

   The truncation parameter m may be tuned specific to the system for addressing cases when paths proceed indefinitely picking up complex roots especially in non-algebraic systems. Paths which are curtailed for the latter two reasons may be pursued along the negative t direction as well before initiating the next iteration.
3. **Iterative Refinement**: The above steps are repeated with different randomly generated $\boldsymbol{\gamma}$ and an updated list of real start points after each iteration. Hence, as more roots are found through the iterations, the number of paths tracked in an iteration also increases progressively. These paths can be tracked simultaneously in a parallel implementation. This process continues until either very few or no new real roots are found for p successive iterations, or a maximum limit of iterations/roots set is reached. For better exploration of the variable space, we reseed a new random complex start point for each iteration using the Newton's method, along with the current set of real start points. We may also tune the magnitude of the elements of the randomly generated vector $\boldsymbol{\gamma}$ as a hyper-parameter to increase the yield. Our numerical experiments demonstrate that increasing the loop size may sometimes improve the yield but at the cost of slower path tracking.

The algorithm proposed here employs a simple strategy for terminating the algorithm based on negligible or zero returns. This approach is computationally efficient but lacks sophistication, yet no better alternatives exist for non-algebraic systems at this time. In the case of polynomial systems with a finite set of isolated roots, a computationally inexpensive second-order local linear trace test [45] exists, which proves sufficient to conclude if all the roots belonging to a numerically irreducible set have been discovered. A termination criterion based on the mark-and-recapture model [39], utilizing likelihood estimates based on diminishing returns, also exists for polynomial systems. Another validation method for determining if all roots within a given variable bound have been found is through the application of multi-variate generalizations of Rouché's theorem [14, p. 153]. For an illustration of this technique in polynomial systems, refer to [46]. However, the challenge lies in the generalization of any such termination criteria to non-algebraic systems while maintaining computational affordability. This is beyond the scope of this work.

3.2. Illustration

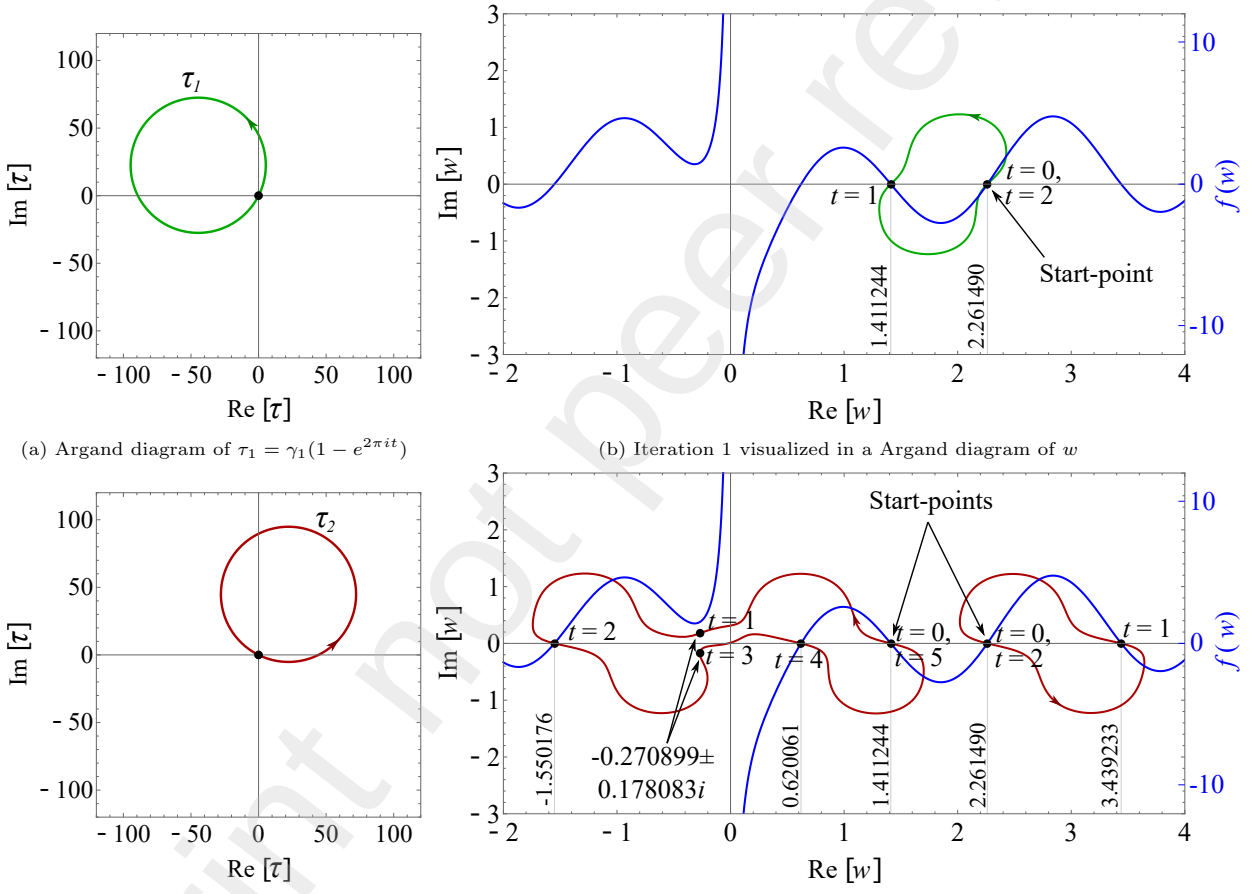

(a) Argand diagram of $\tau_1 = \gamma_1(1 - e^{2\pi i t})$

(b) Iteration 1 visualized in a Argand diagram of w

(c) Argand diagram of $\tau_2 = \gamma_2(1 - e^{2\pi i t})$

(d) Iteration 2 visualized in a Argand diagram of w

Figure 3: Illustration of random monodromy loops algorithm in a 1D root-finding problem

Let us consider a root-finding problem of a non-algebraic equation:

$$f(w) = 0.84 - \frac{1}{w} - \cos[w] - \frac{10}{3}\cos\left[\frac{10w}{3}\right] = 0.$$

This equation represents the stationary points of an objective function taken from [47]. For solving this equation, we construct a homotopy as given by Eq. (12,13). The algorithm is initiated from a real start point $w = 2.261490$ found through Newton's method with an initial guess. During the first iteration, the algorithm uses a randomly generated complex number $\gamma_1 = -44.6510 + 22.5008i$ of magnitude 50. The

corresponding monodromy loop $\tau_1 = \gamma_1(1 - e^{2\pi it})$ is shown as an Argand diagram in Fig. 3a. When $t \in \mathbb{Z}$, $\tau_1 = 0$. The path proceeds from $t = 0$; picks up a new root $w = 1.411244$ at $t = 1$; and completes a circuit by returning to the start point at $t = 2$. This progression is illustrated in Fig. 3b. The real-valued function $f(w)$ is shown as an overlay on the same plot, with scale on the right, for correspondence of the roots of $f(w)$ when $t \in \mathbb{Z}$. The next iteration is initiated with a different random complex number $\gamma_2 = 22.1502 + 44.8260i$, see Fig. 3c. In this case, the two start points found already are seen to follow distinct circuits, each picking up new roots in process before completing the respective circuits as shown in Fig. 3d. Note that the quantity of unique roots within a circuit can vary widely depending on the system and may not be known *a priori*. Furthermore, these roots need not all be real. The supplementary material contains two animations visualizing these iterations. This example showcases that two roots which belong in the same circuit in one monodromy may belong in different circuits in another. Such randomly permuted maps allow the algorithm to proceed and compute new roots efficiently with subsequent iterations. It is worth noting that the function considered has a pole at $w = 0$. Numerical continuation approaches may even be used in some non-analytic functions with isolated poles because the probability of any random path reaching an isolated pole is nearly zero. This is unlike a branch cut, which is not isolated. In the following section, we apply this technique to solve the forward kinematics of CDPRs and benchmark our results against the existing ones from literature.

4. Numerical examples

We solve the forward kinematic problem of an eight-cable system taken from the published data set [29]. This system has an end-effector platform with six DOF which is controlled by eight cables.

4.1. System Specifications and Material Properties

The cable properties are as follows:

$$\rho = 0.079 \text{ kg m}^{-1}, \quad E = 100 \text{ GPa}, \quad A = 0.1256637062 \cdot 10^{-4} \text{ m}^2.$$

Acceleration due to gravity is assumed a constant $g = 9.81$ m s^{-2}. The coordinate points of the cable base points in the global frame and the end-effector points in the local frame are listed in Table 1. The end-effector center of mass is assumed to coincide with the origin of the local frame and it carries $M = 1$ kg. Based on these specifications, the material constants of this system evaluate to $\nu = 0.616717 \cdot 10^{-6}$ m^{-1} and $\lambda = 12.658228$ m. We analyze four distinct data sets, specifically Data Sets $\mathcal{A}$, $\mathcal{B}$, $\mathcal{C}$, and $\mathcal{D}$, which contain unstrained cable lengths for the forward kinematic problem, as listed in Table 2.

Table 1: Coordinate Points for an Eight-Cable Cable-Driven Parallel Robot (CDPR) System

Base Points ($\mathbf{A}_j$, Global Frame)			
Label	x (m)	y (m)	z (m)
$\mathbf{A}_1$	-7.175120	-5.243980	5.462460
$\mathbf{A}_2$	-7.315910	-5.102960	5.472220
$\mathbf{A}_3$	-7.302850	5.235980	5.476150
$\mathbf{A}_4$	7.182060	5.347600	5.488300
$\mathbf{A}_5$	-7.160980	5.372810	5.485390
$\mathbf{A}_6$	7.323310	5.205840	5.499030
$\mathbf{A}_7$	7.301560	-5.132550	5.489000
$\mathbf{A}_8$	7.161290	-5.269460	5.497070

End-Effector Points ($\mathbf{p}_j$, Local Frame)			
Label	x (m)	y (m)	z (m)
$\mathbf{p}_1$	0.503210	-0.492830	0.000000
$\mathbf{p}_2$	-0.509740	0.350900	0.997530
$\mathbf{p}_3$	-0.503210	-0.269900	0.000000
$\mathbf{p}_4$	-0.503210	0.492830	0.000000
$\mathbf{p}_5$	0.496070	0.355620	0.999540
$\mathbf{p}_6$	0.499640	-0.340280	0.999180
$\mathbf{p}_7$	0.502090	0.274900	-0.000620
$\mathbf{p}_8$	-0.504540	-0.346290	0.997520

4.2. Key Considerations and Methodology Details

The forward kinematic problem as per the formulation proposed results in a non-algebraic system of 31 equations in 31 unknowns. For performing monodromy loops, we select the constant parameter space of all the position equations, force and torque equilibrium equations amounting to a dimension of 30, leaving the unit quaternion constraint, Eq. (1). This ensures that the choice of the parameter space coincides with the natural parameter space of the system preserving regularity assumptions of the system as monodromy loops

Table 2: Unstrained Lengths (m) of Eight Cables ($L_j, j = 1, 2, \ldots, 8$) - Four Data Sets ($\mathcal{A}$, $\mathcal{B}$, $\mathcal{C}$, $\mathcal{D}$)

Data Set	L_1	L_2	L_3	L_4	L_5	L_6	L_7	L_8
$\mathcal{A}$	10.538225	11.963397	10.135355	7.703723	10.615617	8.537152	9.969606	8.555879
$\mathcal{B}$	8.306209	7.608231	11.163294	12.406223	11.380175	11.947601	9.495229	8.985027
$\mathcal{C}$	12.192125	11.247648	9.199310	7.929109	8.596630	7.311818	10.839055	10.721407
$\mathcal{D}$	12.924710	11.785460	10.720089	8.037326	10.425254	6.715571	10.163088	9.316678

Table 3: Computational Summary of forward kinematics for a CDPR with eight cables

Data Set	# Iterations	# Real Roots	# Valid Roots ($\alpha_j > \beta_j \ \forall \ j$)	# Valid Roots of Benchmark [29]	Compute Time (hr)
$\mathcal{A}$	207	4306	14	11	2.64
$\mathcal{B}$	117	6717	22	21	3.33
$\mathcal{C}$	105	7301	28	19	3.22
$\mathcal{D}$	394	6119	12	8	3.46

are performed. We do not use the parameter space associated with unstrained cable lengths or the material constant ν for performing monodromy loops as they do not appear in a linear manner in the kineto-static equations. Performing monodromy loops in a parameter space that appears linear can help improve the local conditioning of the system during path tracking.

For the randomly generated numbers used in constructing monodromy loops, we use a magnitude limit of 0.5 for the parameter space corresponding to the position equations and 5 for those corresponding to the force and torque equilibrium equations. These limits were determined through tuning via trial and error. These limits may not be suitable for other problems of varying scales and platform masses and must be tuned accordingly.

Initial guesses for the Newton's method used to find start points are also crucial. The position coordinates of the end-effector can be chosen as complex values within a magnitude limit appropriate for the CDPR operating range's scale. Complex-valued guesses are selected for α and β with a magnitude limit of 10^{-3}, while ϕ is set within a magnitude of π for all cables. Quaternion parameters are chosen to have a unit magnitude.

During monodromy path tracking, as described earlier, we truncate a path if no real root is found for four consecutive instances of the homotopy parameter t crossing an integer. While it is possible that the path might still find a real root if pursued further, we have determined through trial and error that the trade-off between computation time and yield is poor beyond four. The total number of complex roots for this non-algebraic system is theoretically unbounded, and some paths are observed to proceed indefinitely, always landing on complex roots, necessitating this truncation limit.

As for overall algorithm termination criteria, we define the algorithm to terminate when both the yield (percentage increase of real roots) from successive iterations falls below 1% and the number of valid roots remains constant for 10 consecutive iterations. To prevent premature termination, we set a minimum limit of 1000 real roots initially.

4.3. Results

Table 3 reports a summary of the computations performed in the four data sets chosen from [29]. All the computations for each of the four data sets were carried out using the Wolfram Language in Mathematica software [48] on a dual 24-core Intel® Xeon™ 2.30 GHz system in the Center for Research Computing at the University of Notre Dame. In all four cases, the algorithm converged with both the yield of real roots diminishing below 1% and the number of valid roots stalling for 10 consecutive iterations. In all cases, monodromy-based numerical continuation found all the valid roots reported in the existing benchmark set [29] and more. Notably, in Data Sets $\mathcal{C}$ and $\mathcal{D}$, the yield increased by up to 50%. All the valid configurations found are made available to the reader via supplementary material along with their visualizations. For each configuration, the numerical values are reported in the following order: $P_x, P_y, P_z, q_0, q_1, q_2, q_3, \{\alpha_j, \beta_j, \phi_j\}, \ j = 1, 2, \ldots, 8$. Figure 4a illustrates the algorithm's progression across iterations in all four data sets. The initial iterations are computationally inexpensive, and a critical mass of start points is reached before the algorithm acceler-

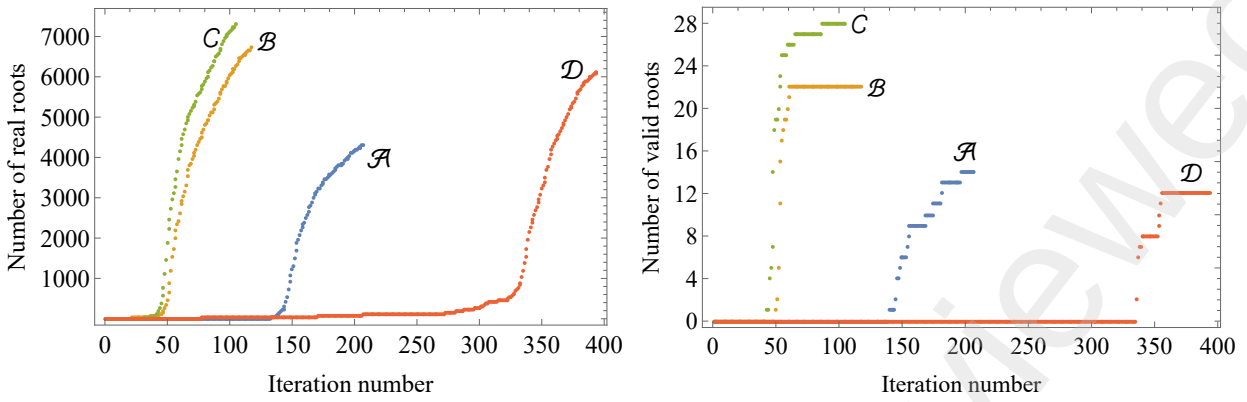

(a) Progression of real roots

(b) Progression of valid roots

Figure 4: Progression of the number of roots plotted against the iterations for the kineto-statics of an eight-cable CDPR

ates in finding real roots as seen in 4a. The point at which this critical mass is reached can vary between runs due to the randomness associated with the technique, and it is not guaranteed to occur at the same iteration number or close. However, because of the low computational cost of the initial iterations, this variability does not pose a significant issue.

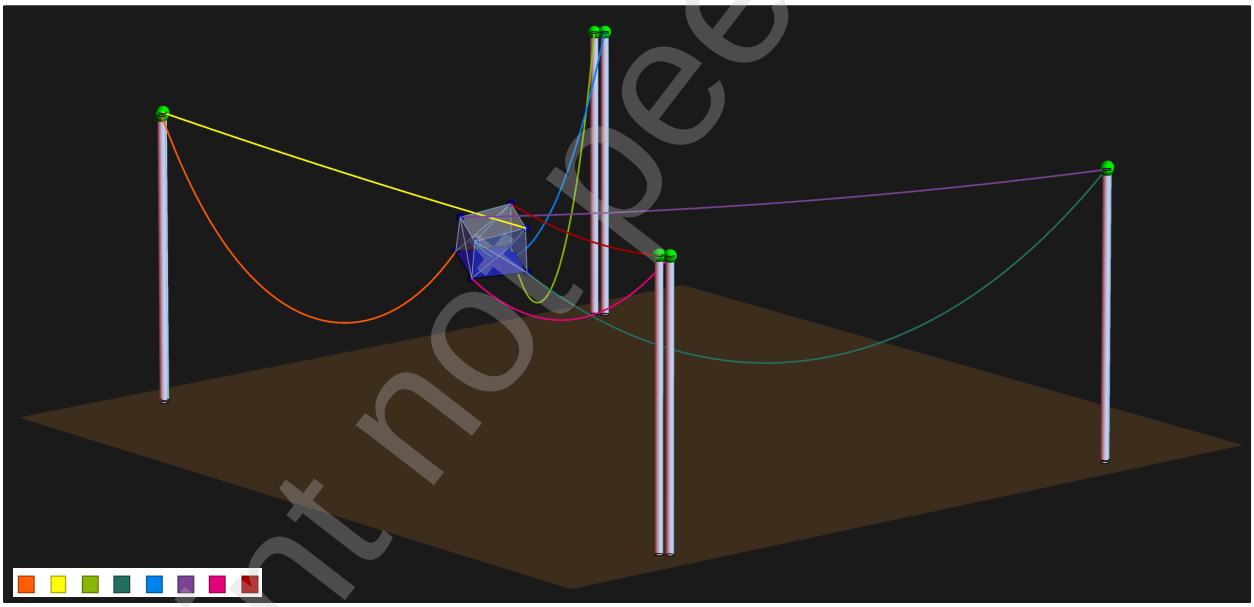

Figure 5: A previously unreported equilibrium configuration (#14) to the forward kinematic problem associated with Data Set $\mathcal{B}$

As mentioned earlier, during the monodromy runs, the inequality condition $\alpha_j > \beta_j \; \forall \; j$ is disregarded. While post-processing after each iteration, we check for this condition to identify the valid roots among the real roots found. Figure 4b records the progression of the number of valid roots against the number of iterations. It illustrates that in Data Set $\mathcal{B}$, all the valid roots are found in just a few iteration sequences. This is because all 22 roots found represent well-behaved configurations close to each other in the variable space, with relatively small tension forces in all the sagging cables. For example, see Fig. 5 for one such configuration. The cable profiles are drawn using Eq. (9). In the other data sets, which contain taut cable configurations with large cable tension forces (see Fig. 6) besides well-behaved ones, the number of valid roots increases in steps with batches of configurations occurring in iteration sequences. This has implications for computation time incurred. For instance, we selected an intensive termination criterion resulting in

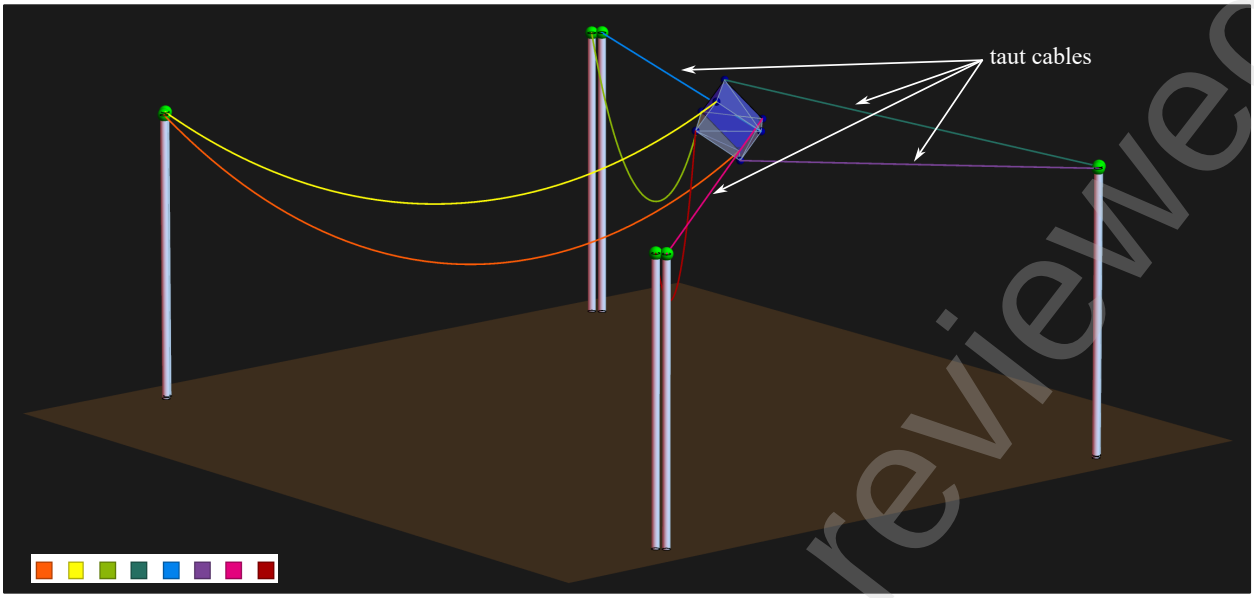

Figure 6: An equilibrium configuration (#16) to the forward kinematic problem associated with Data Set $\mathcal{C}$ with four high tension taut cables

approximately three hours of computation time in each case (see Table 3). However, the majority of well-behaved configurations are discovered within the first hour of computation. Thus, it is important to note that the reported computation time depends on the desired level of diminishing returns.

In Fig. 7, we present a breakdown of all the real roots based on the number of cables in each root that satisfy the valid cable condition $\alpha > \beta$. The numbers indicated correspond to the observed distribution, which is depicted as a histogram in red. The last bar in the histogram signifies the valid roots where all eight cables satisfy this condition. The histogram reveals an intriguing trend: as more real roots are discovered, we observe the emergence of an approximate binomial distribution in all four cases. If one assumes an equal probability $\sigma \in [0, 1]$ for satisfying each valid cable inequality condition in a real root, then the expected binomial probability mass function for a real root having k valid cables is given by

$$P(X = k) = \frac{8!}{k!\,(8-k)!} \cdot \sigma^k \cdot (1-\sigma)^{8-k}, \quad k = 0, 1, \ldots, 8. \tag{14}$$

The binomial distribution in Fig. 7 is not symmetric; in other words, σ skews slightly lower than 0.5 in all four cases, approximately around 0.45. The corresponding expected binomial distributions, derived using a maximum likelihood estimator are shown side-by-side in green in the respective figures. However, it is important to note that a Pearson chi-square goodness-of-fit test yielded significant results, indicating a bad distribution fit, in three out of the four cases, except for the first one when using a one-sided significance level of 0.05 and seven degrees of freedom. This choice of seven degrees of freedom for the chi-square goodness-of-fit test is appropriate due to the estimation of a single parameter, σ, using the maximum likelihood estimator in a scenario with nine categories. It remains to be studied whether this binomial distribution trend occurs across various CDPR systems and whether it can be employed to establish a goodness-of-fit-based termination criterion for the random monodromy loops algorithm applied in the context of global kineto-statics for CDPRs.

5. Properties and Relations

Numerical continuation via monodromy proves to be an effective alternative to interval search-based methods for solving the global kineto-statics of large CDPRs. This method does not require the construction of starting systems, which is typical in classical continuation approaches [28], and can be initiated using a local Newton's method. In terms of computation time, nearly 100% of it is spent on path tracking, with a

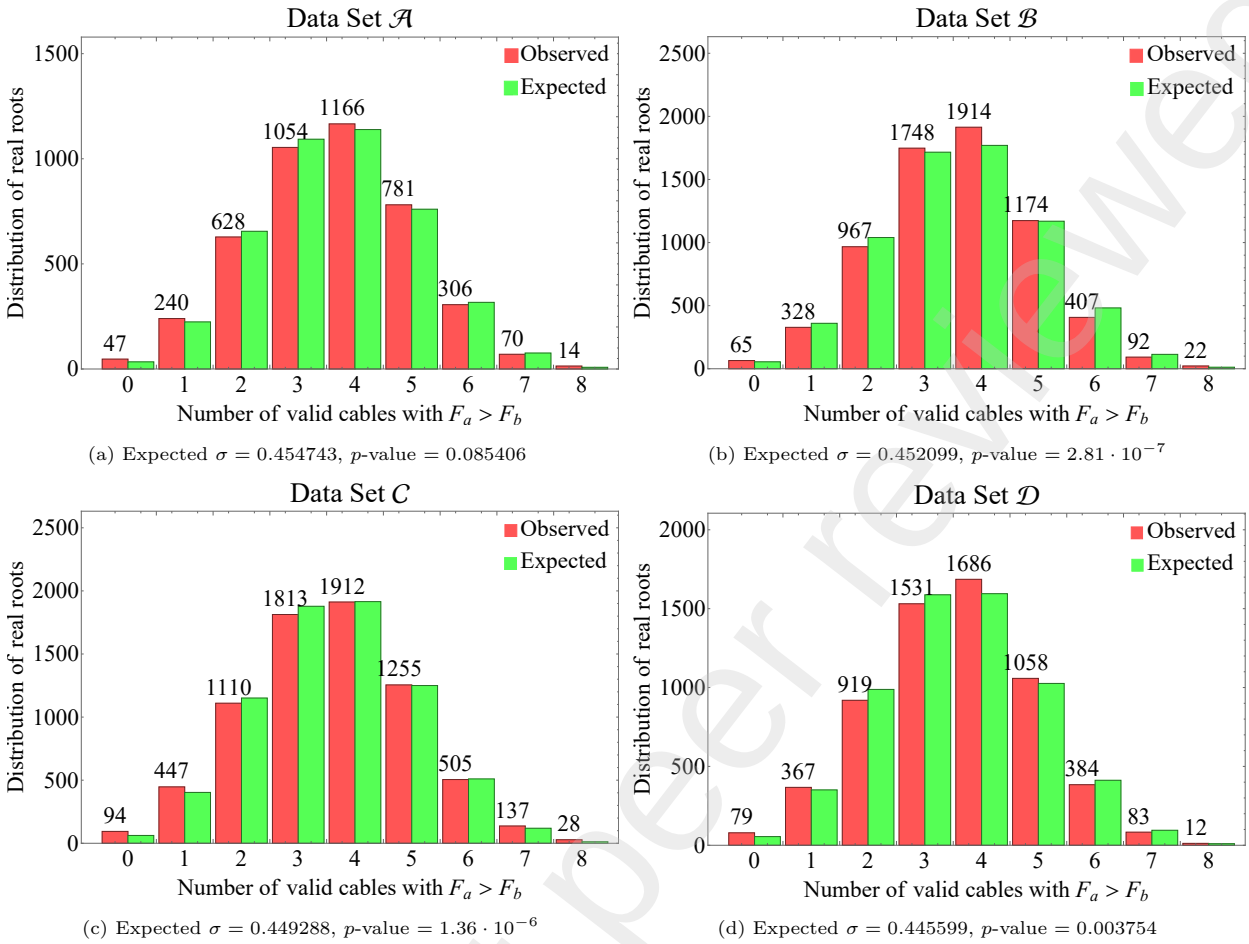

(a) Expected $\sigma = 0.454743$, p-value $= 0.085406$

(b) Expected $\sigma = 0.452099$, p-value $= 2.81 \cdot 10^{-7}$

(c) Expected $\sigma = 0.449288$, p-value $= 1.36 \cdot 10^{-6}$

(d) Expected $\sigma = 0.445599$, p-value $= 0.003754$

Figure 7: Comparison of observed distribution (red) vs. expected distribution (green) of the number of real roots based on the number valid cables within each root

negligible amount allocated to data processing. Therefore, improving path tracking routines and implementing efficiency enhancements can further reduce computation time. Smarter root accumulation strategies that promptly discard sufficiently explored start points as the iterations progress may also be considered. This approach can help reduce computation time instead of retaining all the real roots indiscriminately.

The primary focus of this method is not to provide a real-time routine but to offer a robust way to discover all possible configurations for a handful of unstrained cable lengths. This will facilitate the generation of training and test data sets of workspace points in conjunction with local parameter continuation methods. Ultimately, this will aid in the creation of large neural network models that may be useful for real-time implementation [20]. In this regard, the current work is similar in scope to previous studies [22, 28].

Interval search methods in these large cable systems encounter the 'curse of dimensionality', especially when expanding the search bounds. Unlike these methods, the numerical continuation approach we present here does not face this issue because monodromy loops can seamlessly traverse the variable space. The dimensionality problem takes a different form in the shape of invalid real roots which violate the cable inequality condition $\alpha > \beta$. As a rule of thumb, for an n-cable system, one can generally expect that only a small fraction of 2^{-n} of the real roots will be valid when assuming a 0.5 probability for a real root to satisfy each valid cable inequality condition. However, this is a trade-off we must accept because during monodromy runs, real roots may transition from invalid to valid and vice versa. While observing diminishing returns in the total number of real roots, including invalid ones, found over the iterations can provide some insights into the near completeness of the solution set, determining the data set's completeness requires further investigation. In any case, our benchmarking demonstrates that numerical continuation uncovers up to 50%

more valid roots than previously reported in literature. Consequently, our approach has the potential to enhance the quality of the data sets needed to construct large neural network models for the kineto-statics of CDPRs.

6. Conclusion

We present a numerical continuation method to solve the global forward kineto-statics of large CDPRs with sagging cables. As a first step, we reformulate the popular Irvine cable model to remove all multi-valued functions, enabling effective analytical continuation for studying these systems. This new kineto-static model depends on two consolidated material constants, in addition to the geometric parameters, and offers computational advantages for modeling and solving CDPR systems with large tension forces in the cables. Next, we propose a novel heuristic strategy for root accumulation, utilizing random monodromy loops in an iterative approach to find roots in nonlinear, non-algebraic, and complex-analytic systems. This strategy involves tracking circuits while performing monodromy loops instead of following lone paths, potentially identifying multiple roots in the process. The rationale behind this approach is that multiple valid roots are often closely located in the variable space, and this approach can efficiently uncover them. We employ a termination criterion based on diminishing returns across iterations. With this approach, we successfully solve the global kineto-static problem of an eight-cable spatial CDPR system. In some numerical examples, we observe an increase in yields of up to 50% compared to existing data sets in literature. This method is expected to augment existing local parameter continuation methods, improving the quality of data sets used to train and test large neural network models for the kineto-statics of CDPRs with sagging cables.

Acknowledgment

The first author was supported in part from Wolfram Research, Inc., and, in particular, acknowledge mentorship from Daniel Lichtblau. The first three authors were supported in part by NSF CMMI 2041789. The last author was supported in part by the Huisking Foundation, Inc.

References

[1] E. Barnett, C. Gosselin, Large-scale 3D printing with a cable-suspended robot, Additive Manufacturing 7 (2015) 27–44.

[2] J. Merlet, Y. Papegay, The new exhibition blind machines, a large 3D printing machine, in: 2023 IEEE International Conference on Robotics and Automation (ICRA), IEEE, 2023, pp. 9721–9727.

[3] J.-B. Izard, A. Dubor, P.-E. Hervé, E. Cabay, D. Culla, M. Rodriguez, M. Barrado, Large-scale 3D printing with cable-driven parallel robots, Construction Robotics 1 (2017) 69–76.

[4] J.-P. Merlet, Marionet, a family of modular wire-driven parallel robots, in: Advances in Robot Kinematics: Motion in Man and Machine: Motion in Man and Machine, Springer, 2010, pp. 53–61.

[5] R. G. Roberts, T. Graham, T. Lippitt, On the inverse kinematics, statics, and fault tolerance of cable-suspended robots, Journal of Robotic Systems 15 (10) (1998) 581–597.

[6] M. Carricato, J.-P. Merlet, Stability analysis of underconstrained cable-driven parallel robots, IEEE Transactions on Robotics 29 (1) (2012) 288–296.

[7] H. M. Irvine, Cable structures, The MIT Press Series in Structural Mechanics, 1981.

[8] J.-P. Merlet, Some properties of the Irvine cable model and their use for the kinematic analysis of cable-driven parallel robots, Mechanism and Machine Theory 135 (2019) 271–280.

[9] E. Stump, V. Kumar, Workspaces of Cable-Actuated Parallel Manipulators, Journal of Mechanical Design 128 (1) (2005) 159–167.

[10] G. Abbasnejad, M. Carricato, Direct geometrico-static problem of underconstrained cable-driven parallel robots with n cables, IEEE Transactions on Robotics 31 (2) (2015) 468–478.

[11] A. Berti, J.-P. Merlet, M. Carricato, Solving the direct geometrico-static problem of underconstrained cable-driven parallel robots by interval analysis, The International Journal of Robotics Research 35 (6) (2016) 723–739.

[12] K. Kozak, Q. Zhou, J. Wang, Static analysis of cable-driven manipulators with non-negligible cable mass, IEEE Transactions on Robotics 22 (3) (2006) 425–433.

[13] J.-P. Merlet, R. Tissot, A panorama of methods for dealing with sagging cables in cable-driven parallel robots, in: International Symposium on Advances in Robot Kinematics, Springer, 2022, pp. 122–130.

[14] L. V. Ahlfors, Complex analysis, McGraw-Hill, Inc., 1979.

[15] P. B. Edwards, A. Baskar, C. Hills, M. Plecnik, J. D. Hauenstein, Output mode switching for parallel five-bar manipulators using a graph-based path planner, in: 2023 IEEE International Conference on Robotics and Automation (ICRA), 2023, pp. 9735–9741.

[16] C. Gosselin, J. Angeles, Singularity analysis of closed-loop kinematic chains., IEEE transactions on robotics and automation 6 (3) (1990) 281–290.

[17] M. Urizar, V. Petuya, O. Altuzarra, A. Hernandez, Computing the configuration space for motion planning between assembly modes, in: Computational Kinematics: Proceedings of the 5th International Workshop on Computational Kinematics, Springer, 2009, pp. 35–42.

[18] S. Briot, J.-P. Merlet, Direct kinematic singularities and stability analysis of sagging cable-driven parallel robots, IEEE Transactions on Robotics (2023).

[19] I. Chawla, P. Pathak, L. Notash, A. Samantaray, Q. Li, U. Sharma, Inverse and forward kineto-static solution of a large-scale cable-driven parallel robot using neural networks, Mechanism and Machine Theory 179 (2023) 105107.

[20] J.-P. Merlet, Advances in the use of neural network for solving the direct kinematics of CDPR with sagging cables, in: International Conference on Cable-Driven Parallel Robots, Springer, 2023, pp. 30–39.

[21] A. Khovanskii, Fewnomials and Pfaff manifolds, in: Proceedings of the International Congress of Mathematicians, Vol. 1, 1983, p. 2.

[22] J.-P. Merlet, J. Alexandre-dit Sandretto, The forward kinematics of cable-driven parallel robots with sagging cables, in: Cable-Driven Parallel Robots: Proceedings of the Second International Conference on Cable-Driven Parallel Robots, Springer, 2015, pp. 3–15.

[23] D. J. Bates, A. J. Sommese, J. D. Hauenstein, C. W. Wampler, Numerically solving polynomial systems with Bertini, SIAM, 2013.

[24] D. J. Bates, J. D. Hauenstein, A. J. Sommese, C. W. Wampler, Bertini: Software for numerical algebraic geometry.

[25] H. Tari, H.-J. Su, J. D. Hauenstein, Classification and complete solution of the kinetostatics of a compliant Stewart–Gough platform, Mechanism and Machine Theory 49 (2012) 177–186.

[26] D. Mehta, T. Chen, J. D. Hauenstein, D. J. Wales, Communication: Newton homotopies for sampling stationary points of potential energy landscapes, The Journal of chemical physics 141 (12) (2014).

[27] M. M. Plecnik, The kinematic design of six-bar linkages using polynomial homotopy continuation, University of California, Irvine, 2015.

[28] J.-P. Merlet, A generic numerical continuation scheme for solving the direct kinematics of cable-driven parallel robot with deformable cables, in: 2016 IEEE/RSJ International Conference on Intelligent Robots and Systems (IROS), IEEE, 2016, pp. 4337–4343.

[29] J.-P. Merlet, Data base for the direct kinematics of cable-driven parallel robot (CDPR) with sagging cables (2021).

[30] C. W. Wampler, A. P. Morgan, A. J. Sommese, Complete Solution of the Nine-Point Path Synthesis Problem for Four-Bar Linkages, Journal of Mechanical Design 114 (1) (1992) 153–159.

[31] J. D. Hauenstein, L. Oeding, G. Ottaviani, A. J. Sommese, Homotopy techniques for tensor decomposition and perfect identifiability, Journal für die reine und angewandte Mathematik (Crelles Journal) 2019 (753) (2019) 1–22.

[32] E. L. Allgower, K. Georg, Numerical continuation methods: an introduction, Vol. 13, Springer Science & Business Media, 2012.

[33] J. Verschelde, P. Verlinden, R. Cools, Homotopies exploiting Newton polytopes for solving sparse polynomial systems, SIAM Journal on Numerical Analysis 31 (3) (1994) 915–930.

[34] B. Huber, B. Sturmfels, A polyhedral method for solving sparse polynomial systems, Math. Comp. 64 (212) (1995) 1541–1555.

[35] M. M. Plecnik, J. Michael McCarthy, Computational design of Stephenson II six-bar function generators for 11 accuracy points, Journal of Mechanisms and Robotics 8 (1) (2016) 011017.

[36] M. M. Plecnik, R. S. Fearing, Finding only finite roots to large kinematic synthesis systems, Journal of Mechanisms and Robotics 9 (2) (2017) 021005.

[37] A. Baskar, S. Bandyopadhyay, An algorithm to compute the finite roots of large systems of polynomial equations arising in kinematic synthesis, Mechanism and Machine Theory 133 (2019) 493–513.

[38] T. Duff, C. Hill, A. Jensen, K. Lee, A. Leykin, J. Sommars, Solving polynomial systems via homotopy continuation and monodromy, IMA Journal of Numerical Analysis 39 (3) (2019) 1421–1446.

[39] J. D. Hauenstein, S. N. Sherman, Using monodromy to statistically estimate the number of solutions, in: 2nd IMA Conference on Mathematics of Robotics (2020), Vol. 21, Springer Proceedings in Advanced Robotics, 2022, pp. 37–46.

[40] A. Baskar, M. Plecnik, Synthesis of six-bar timed curve generators of Stephenson-type using random monodromy loops, Journal of Mechanisms and Robotics 13 (1) (2021) 011005.

[41] J. D. Hauenstein, A. C. Liddell Jr, Certified predictor–corrector tracking for Newton homotopies, Journal of Symbolic Computation 74 (2016) 239–254.

[42] HomotopyContinuation.jl, Solving parametrized systems with monodromy - Strategies, accessed: 2023-10-23.

[43] S. Timme, Mixed precision path tracking for polynomial homotopy continuation, Advances in Computational Mathematics 47 (5) (2021) 75.

[44] S. Telen, M. V. Barel, J. Verschelde, A robust numerical path tracking algorithm for polynomial homotopy continuation, SIAM Journal on Scientific Computing 42 (6) (2020) A3610–A3637.

[45] D. A. Brake, J. D. Hauenstein, A. C. Liddell Jr, Decomposing solution sets of polynomial systems using derivatives, in: International Congress on Mathematical Software, Springer, 2016, pp. 127–135.

[46] J. Verschelde, A. Haegemans, Homotopies for solving polynomial systems within a bounded domain, Theoretical computer science 133 (1) (1994) 165–185.

[47] L. Timonov, An algorithm for search of a global extremum, Engineering Cybernetics 15 (3) (1977) 38–44.

[48] Wolfram Research Inc., Mathematica, Version 13.2.0.0, Champaign, IL, 2023.